Extended Abstracts of the 2010 International Conference on Solid State Devices and Materials, Tokyo, 2010, pp1307-1308

K-8-5

Strain-Induced Back Channel Electron Mobility Enhancement in Poly-Si TFTs Formed by Continuous-Wave Laser Lateral Crystallization

Shuntaro Fujii, Shin-Ichiro Kuroki, Koji Kotani, and Takashi Ito

Graduate School of Engineering, Tohoku University
6-6-05, Aza-Aoba, Aramaki, Aoba-ku, Sendai 980-8579, Japan
Phone: +81-22-795-7122, Fax: +81-22-263-9396, E-mail: {sfujii, kuroki}@ecei.tohoku.ac.jp

1. Introduction

High performance poly-Si TFTs with high carrier mobility are expected for a system on glass application. To enhance the mobility, various laser crystallization processes to enlarge grain size have been developed [1-5]. Among them, continuous-wave (CW) laser lateral crystallization (CLC) can form the longest grains [3-5]. It has been found that CLC poly-Si films have tensile strain [4, 5]. However, the strain effect to the mobility has not been clarified yet although strain modulates mobility [6]. In this study, 4-terminal (4T) CLC poly-Si TFTs having both front and back gates were fabricated and the strain effect was investigated by comparing front channel mobility ($\mu_{eff,\ front}$) with back channel mobility ($\mu_{eff,\ back}$).

2. Experiments

Figure 1 shows the process flow. In CLC (λ=532 nm), the laser spot size was 90×20 μm^2 (FWHM) with a Gaussian profile. Figure 2 shows cross-sectional schematic images of the CLC poly-Si TFTs. For comparison, 3-terminal (3T) CLC poly-Si TFTs (front channel operation, not having back gates) were also fabricated. The channel direction was parallel to the laser scanning direction. Both the gate length (L) and gate width (W) were 10 μm. Both the front gate oxide thickness (T_{FOX}) and back gate oxide thickness (T_{BOX}) were 200 nm. The channel poly-Si thickness (T_{Si}) was 150 nm.

3. Results and discussions

Figure 3 shows the electron backscattered diffraction (EBSD) mappings of the channel poly-Si films. Lateral crystallization was achieved even if the stacked Si films were simultaneously annealed by a CW green laser. The average grain length was 20 μm. Figure 4 shows the average $\mu_{eff,\ front}$ (μ) and its standard deviation (σ) at the inversion carrier density (N_{inv}) of 5×10^{12} cm^{-2} and temperature (T) of 293K. μ and σ in 4T CLC poly-Si TFTs were 333 and 53 $cm^2/(V \cdot s)$, respectively. μ and σ in 3T CLC poly-Si TFTs were also shown. Noticeable difference was not observed. Figure 5 shows the typical characteristics of $\mu_{eff,\ front}$ dependence on N_{inv}. As T increased, $\mu_{eff,\ front}$ was proportional to $N_{inv}^{-0.3}$. This results shows that $\mu_{eff,\ front}$ was mainly governed by mobility limited by phonon scattering [7]. From these results, it was confirmed that the crystalline quality of the channel poly-Si films in 4T CLC poly-Si TFTs was comparable with that in 3T CLC poly-Si TFTs. Then, the strain effect to the mobility was investigated by analyzing 4T CLC poly-Si TFTs.

Figure 6 shows the (111) peak 2θ dependence on the incident angle in X-ray diffraction (XRD) measurement in the in-plane direction. As the incident angle increased, the peak 2θ decreased. This result shows that the back interface had larger tensile strain than the surface. The strain values at the surface and back interfaces were estimated at ~0.3% and 0.4% or larger, respectively. Figures 7(a) and 7(b) show the I_D-V_{GS} characteristics of 4T CLC poly-Si TFTs in front and back channel operation, respectively. V_{th} (V_{GS} at $I_D=1\times10^{-7}$ A) was controlled by V_{BACK} or V_{FRONT}. Figure 8 shows V_{th} dependence on V_{BACK} or V_{FRONT}. The slopes in Fig. 8 showed the body factor (γ). In both front and back channel operation, $\gamma_{Standby}$ and γ_{Active} were 0.8 and 1.2 V/V, respectively. In the case of $T_{FOX}=T_{BOX}=T_{OX}$, $\gamma_{Standby}$ and γ_{Active} in 4T MOSFETs are expressed as $3T_{OX}/(3T_{OX}+T_{Si})$ and $(3T_{OX}+T_{Si})/3T_{OX}$, respectively [8]. In this study, theoretical values of $\gamma_{Standby}$ and γ_{Active} were 0.80 and 1.25 V/V, respectively. Successful operation of variable V_{th} scheme in both front and back channel operation was achieved. To comparing $\mu_{eff,\ front}$ with $\mu_{eff,\ back}$, 4T CLC poly-Si TFTs were biased into a standby state so as not to form the inversion layer on the V_{th}-control gate side. Figure 9 shows typical characteristics of $\mu_{eff,\ front}$ and $\mu_{eff,\ back}$ dependences on N_{inv}. $\mu_{eff,\ back}$ was larger than $\mu_{eff,\ front}$. Figure 10 shows the relationship between $\mu_{eff,\ front}$ and $\mu_{eff,\ back}$. The enhancement factor ($\mu_{eff,\ back}/\mu_{eff,\ front}$) was 1.2, which was comparable with that in strained SOI MOSFETs [9]. It was found that the larger tensile strain around back interface enhanced $\mu_{eff,\ back}$.

4. Conclusions

4T CLC poly-Si TFTs were fabricated to investigate the effect of tensile strain induced by CLC. The strain values at the surface and back interfaces were estimated at ~0.3% and 0.4% or larger, respectively. Because of the larger tensile strain, $\mu_{eff,\ back}$ was 1.2 times larger than $\mu_{eff,\ front}$. Back channel operation in CLC poly-Si TFTs is useful for enhancing the CLC poly-Si TFT performance.

Acknowledgements

A part of this work was supported by Grant-in-Aid for JSPS Fellows (21・2930).

References

[1] S. Miyano et al: JJAP **48** (2009) 03B013. [2] V. Rana et al: IEEE TED **52** (2005) 2622. [3] A. Hara et al: JJAP **43** (2004) 1269. [4] S. Fujii et al: JJAP **47** (2008) 3046. [5] S. Fujii et al: JJAP **48** (2009) 04C129. [6] S. Takagi et al: JAP **80** (1996) 1567. [7] S. Takagi et al: IEEE TED **41** (1994) 2357. [8] M. Masahara et al: IEEE TED **52** (2005) 2046. [9] T. Mizuno et al: IEEE TED **50** (2003) 988.

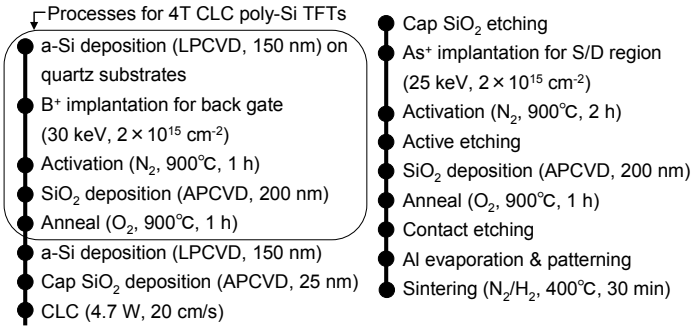

Fig. 1 Process flow.

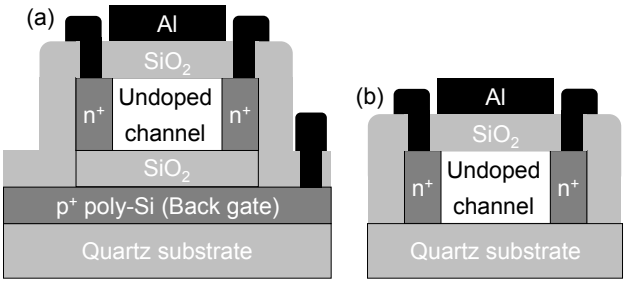

Fig. 2 Cross-sectional schematic images. (a) 4T CLC poly-Si TFT. (b) 3T CLC poly-Si TFT.

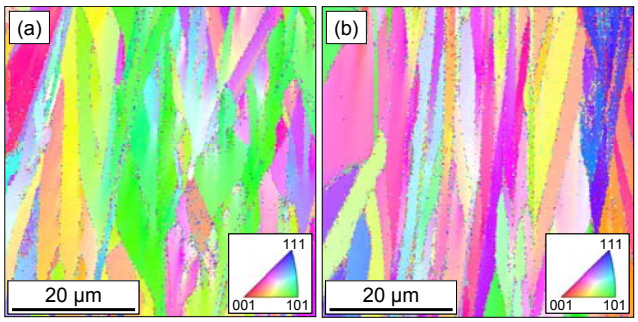

Fig. 3 EBSD mappings of the channel poly-Si films. (a) 4T CLC poly-Si TFT. (b) 3T CLC poly-Si TFT.

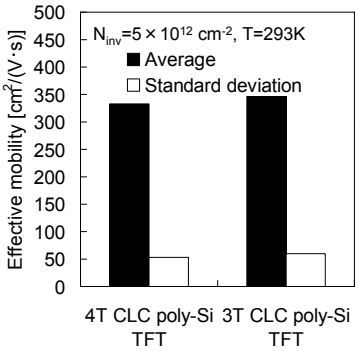

Fig. 4 Average $\mu_{eff,\ front}$ and its standard deviation.

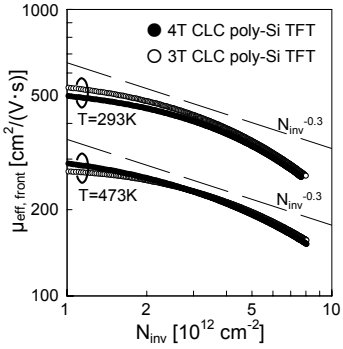

Fig. 5 Typical characteristics of $\mu_{eff,\ front}$ dependence on N_{inv}.

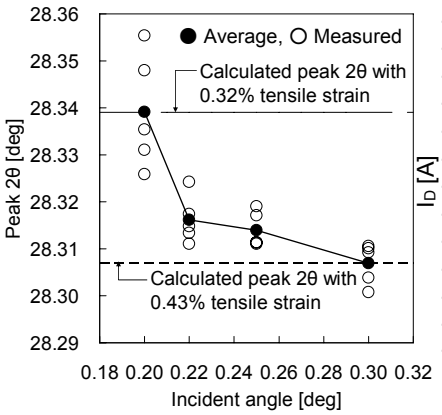

Fig. 6 (111) peak 2θ dependence on the incident angle in XRD measurement in in-plane direction.

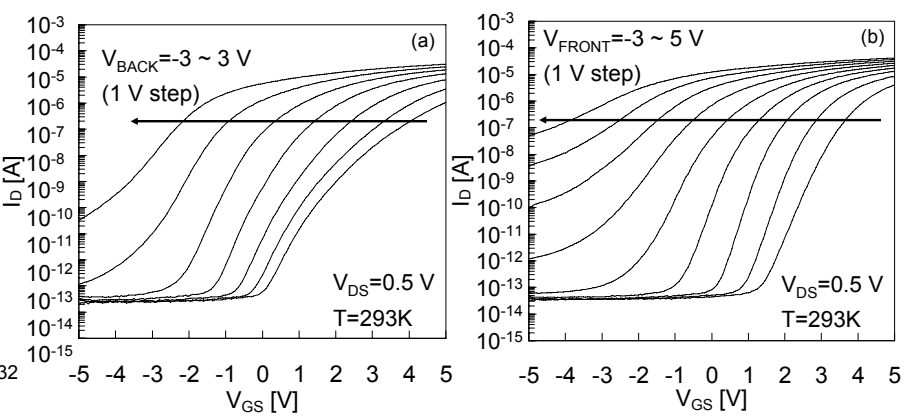

Fig. 7 I_D-V_{GS} characteristics of 4T CLC poly-Si TFT. (a) Front channel operation. (b) Back channel operation.

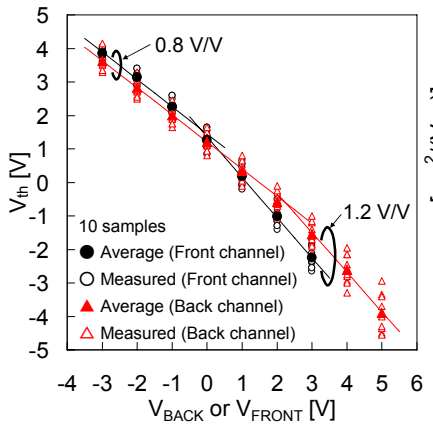

Fig. 8 V_{th} dependence on V_{BACK} or V_{FRONT}.

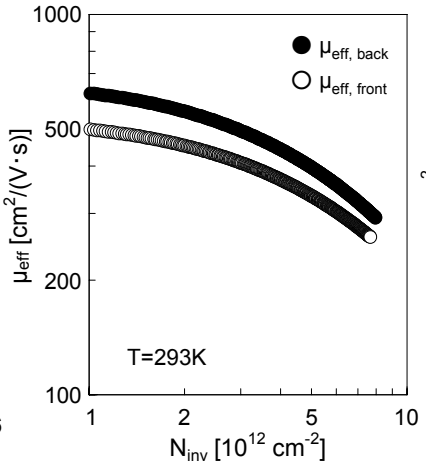

Fig. 9 Typical characteristics of $\mu_{eff,\ back}$ and $\mu_{eff,\ front}$ dependences on N_{inv}.

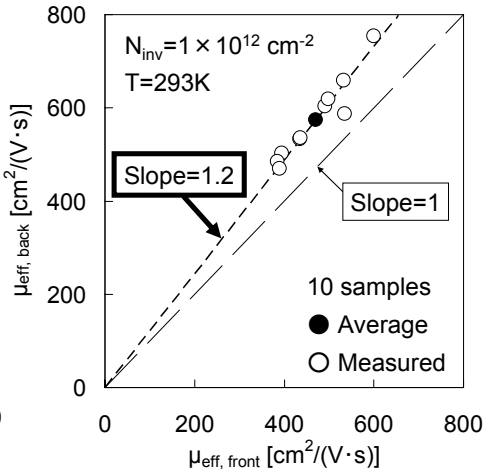

Fig. 10 Relationship between $\mu_{eff,\ front}$ and $\mu_{eff,\ back}$.